













Modeling of the Electrical Characteristics and Degradation Mechanisms of UV-C LEDs

Nicola Roccato , *Graduate Student Member, IEEE*, Francesco Piva , *Associate Member, IEEE*, Carlo De Santi , *Member, IEEE*, Matteo Buffolo , *Member, IEEE*, Normal Susilo, Daniel Hauer Vidal , Anton Muhin , Luca Sulmoni , Tim Wernicke , Micheal Kneissl , *Fellow, IEEE*, Gaudenzio Meneghesso , *Fellow, IEEE*, Enrico Zanoni , *Life Fellow, IEEE*, and Matteo Meneghini , *Senior Member, IEEE*

Abstract—In this paper we investigate the reliability of AlGaIn-based UV-C LEDs with an emission wavelength of 265 nm. By submitting the devices to constant current stress, two main electrical degradation processes are identified: a turn-on voltage shift and an increase in the forward leakage current. In particular, these processes were respectively attributed to: (i) a partial passivation of the Mg-doping concentration in the region adjacent to the contact, probably caused by a local hydrogen diffusion, and ii) a diffusion/generation process of defects in the interlayer, responsible for the increase in the trap-assisted tunneling. To validate these hypotheses, we employed TCAD simulations by varying only the Mg-doping concentration in the region adjacent to the p-contact and the defect density in the interlayer. Thus, we correctly reproduced the experimental variation in electrical characteristics, confirming the physical mechanisms identified.

Index Terms—UV-C, Light-Emitting Diodes, Trap-assisted tunneling (TAT), degradation, modeling, defects, diffusion.

I. INTRODUCTION

THE use of UV-C light-emitting diodes (LEDs) can provide several advantages for many applications, such as disinfection, curing, gas sensing and skin safe disinfection [1], [2], [3], [4], [5], [6]. Compared to conventional UV sources, these devices are more compact, more efficient, free from mercury, have faster switching speed and do not require a warm-up time [7]. Despite that, such devices still exhibit different issues, both in terms of efficiency and reliability, that limit their spread into

Manuscript received 1 December 2023; revised 2 January 2024; accepted 12 January 2024. Date of publication 18 January 2024; date of current version 1 February 2024. This work was supported in part by the National Recovery and Resilience Plan, Mission 4, Component C2, Investment 1.1 and in part by the European Union – NextGenerationEU. PRIN Project 20225YYLEP, "Empowering UV Led technologies for high-efficiency disinfection: from semiconductor-level research to SARS-Cov-2 inactivation. (Corresponding author: Nicola Roccato.)

Nicola Roccato, Francesco Piva, Carlo De Santi, Matteo Buffolo, Gaudenzio Meneghesso, and Enrico Zanoni are with the Department of Information Engineering, University of Padova, 35131 Padova, Italy (e-mail: roccatonic@dei.unipd.it).

Normal Susilo, Daniel Hauer Vidal, Anton Muhin, Luca Sulmoni, and Tim Wernicke are with the Technische Universität Berlin, Institute of Solid State Physics, 10623 Berlin, Germany.

Micheal Kneissl is with the Technische Universität Berlin, Institute of Solid State Physics, 10623 Berlin, Germany, and also with the Ferdinand-Braun-Institut, 12489 Berlin, Germany.

Matteo Meneghini is with the Department of Information Engineering, University of Padova, 35131 Padova, Italy, and also with the Department of Physics and Astronomy, University of Padova, 35131 Padova, Italy.

Digital Object Identifier 10.1109/JPHOT.2024.3355553

the market [8], [9]. In particular, during ageing they exhibit a significant optical and electrical degradation that negatively impacts on their performance [10], [11]. In this paper, we investigate the degradation mechanisms that worsen the electrical characteristics of these devices. In particular, after an experimental accelerated lifetime test on a 265 nm UV-C LED, we identified two main degradation processes: a turn-on voltage shift and an increase in the leakage current. These processes were modeled by means of numerical TCAD simulations, which allowed us to reproduce the experimentally-observed variations in the I-V curve, and to pinpoint their physical origin.

II. EXPERIMENTAL INVESTIGATION

In this study, we investigated AlGaIn-based UV-C LEDs featuring a peak emission wavelength of 265 nm and an area of 10^{-3}cm^{-2} . The devices are grown by metalorganic vapor phase epitaxy (MOVPE) on high-temperature annealed (HTA) epitaxially laterally overgrown (ELO) AlN on sapphire, with a threading dislocation density of $9 \times 10^8 \text{cm}^{-2}$ [12].

The active region consists of a single $\text{Al}_{0.48}\text{Ga}_{0.52}\text{N}$ quantum well (QW), placed between a Si-doped $\text{Al}_{0.62}\text{Ga}_{0.38}\text{N}$ first barrier ($N_D = 5 \times 10^{18}\text{cm}^{-3}$), whose thickness is 38 nm, and a 10 nm thick undoped last barrier (LB), with the same molar concentration. The first barrier (FB) is grown on a 200 nm Si-doped $\text{Al}_{0.65}\text{Ga}_{0.35}\text{N}$ contact layer ($N_D = 4 \times 10^{18}\text{cm}^{-3}$). Over the last barrier, instead, an undoped $\text{Al}_{0.8}\text{Ga}_{0.2}\text{N}$ interlayer divides the p-side from the active region, followed by an electron blocking layer (EBL) composed by Mg-doped ($N_A = 1 \times 10^{19}\text{cm}^{-3}$) $\text{Al}_{0.75}\text{Ga}_{0.25}\text{N}$. Finally, a 230 nm Mg-doped GaN contact layer ($N_A = 6 \times 10^{19}\text{cm}^{-3}$) completes the structure, with a Pd/Au metallization deposited as p-electrode [13]. A schematic representation of the structure is reported in Fig. 1.

In order to evaluate the degradation processes of the devices, constant current stress tests were carried out at 100A/cm^2 (100 mA) for more than 300 h (19000 min). Fig. 2 reports the electrical characteristics before and after the stress. As highlighted, we can split the I-V curve of the LED in two main regions: (a) the forward bias region (in green), and (b) the sub-turn on region (in red). In region (a) the forward conduction of the p-n junction is limited by the effects of the equivalent series resistance, which can be associated to the resistivity of

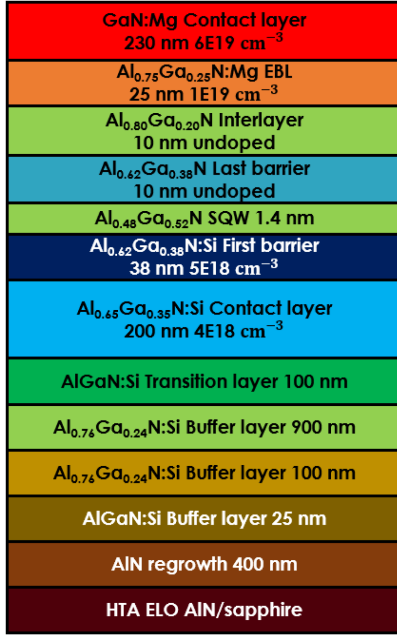


Fig. 1. Schematic representation of the epitaxial structure of the LED.

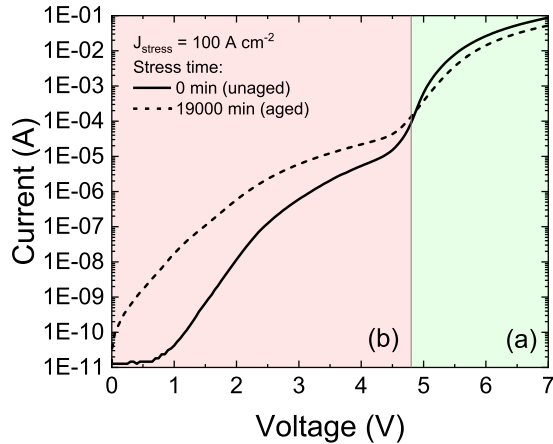


Fig. 2. Comparison between the electrical characteristic of the device before and after the ageing test. Two different regions can be identified: (a) the forward bias region and (b) the sub-turn on region.

the layers and contacts, potential barriers or poor injection at the contact [8], [9]. After stress we can observe a shift in the turn-on voltage toward higher voltages, and a slight increase in the equivalent series resistance.

In region (b) the electrical characteristic is dominated by trap assisted tunneling (TAT)-related forward leakage current [14]. In this case, current conduction is assisted by the presences of deep defects located within the space charge region, which can help carriers tunnel and recombine non-radiatively through the active region [15]. Fig. 2 shows an increase in the forward leakage current after stress, which was therefore associated to an increase in trap concentration in the depletion region during the ageing test [16].

TABLE I
MAIN PARAMETERS ADOPTED FOR THE TCAD SIMULATIONS

| Parameter | 0 min | 19000 min |
|------------------|------------------------------------|---------------------------------------|
| [Si] | $E_C - 24 \text{ meV}$ | $E_C - 24 \text{ meV}$ |
| [Mg] in GaN | $E_V + 150 \text{ meV}$ | $E_C + 150 \text{ meV}$ |
| [Mg] in EBL | $E_V + 380 \text{ meV}$ | $E_V + 380 \text{ meV}$ |
| E_T level | $E_C - 3.5 \text{ eV}$ | $E_C - 3.5 \text{ eV}$ |
| N_T in EBL/IL | $1 \times 10^{16} \text{ cm}^{-3}$ | $7 \times 10^{17} \text{ cm}^{-3}$ |
| N_T in IL/LB | $1 \times 10^{15} \text{ cm}^{-3}$ | $1 \times 10^{16} \text{ cm}^{-3}$ |
| m_{TAT} | $0.07 m_0$ | $0.07 m_0$ |
| $m_{contact}$ | $0.15 m_0$ | $0.15 m_0$ |
| R_p | $4 \times 10^{10} \Omega$ | $5 \times 10^8 \Omega$ |
| R_s | 11Ω | 13.7Ω |
| p-doping contact | $6 \times 10^{19} \text{ cm}^{-3}$ | $4.85 \times 10^{19} \text{ cm}^{-3}$ |

To reproduce the variations exhibited by the electrical characteristics during ageing, we created a model of the device, by implementing the structure through the Sentaurus suite, available from Synopsys. The doping of the layers has been implemented by including the donor or acceptor species as traps (Si and Mg) with their respective characteristic thermal activation energies [17], [18], [19]. All the details are reported in Table I. The recombination coefficients of radiative, SRH and Auger-Meitner rates are set at $2 \times 10^{-10} \text{ cm}^3/\text{s}$, $2 \times 10^7 \text{ s}^{-1}$ and $1 \times 10^{-30} \text{ cm}^6/\text{s}$ respectively, based on typical values found in the literature for similar devices [20], [21], [22], [23]. An additional shunt resistance was added to the model to consider the impact of parasitic conduction paths at very low voltages [24], that show an ohmic behavior [25], [26] whereas a discrete series resistance was added to reproduce additional non-idealities of the contact, buffer layers or partial activation of doping [30] not considered by our simulation framework. The values of both parameters were chosen based on their extrapolation from the experimental I-V characteristics.

III. MODELING OF P-CONTACT DEGRADATION

As mentioned before, ageing induced a shift in the turn-on voltage and a slight increase in series resistance. The former process can typically be ascribed to a partial passivation of magnesium close to the p-contact [27], [28]. The inactivation of Mg-doping can be physically justified by a local migration of hydrogen, which can bond with Mg-acceptors, passivate them, and reduce the acceptor density near the contact on the p-side [22]. This causes a broadening of the space charge region at the p-contact, decreasing in the tunneling probability for the holes. This ultimately lowers the carrier injection at a given voltage. This hypothesis has widely investigated in this work [27], where the effects on the electrical characteristic have been measured, and hydrogen has been supposed to be responsible for Mg passivation [29].

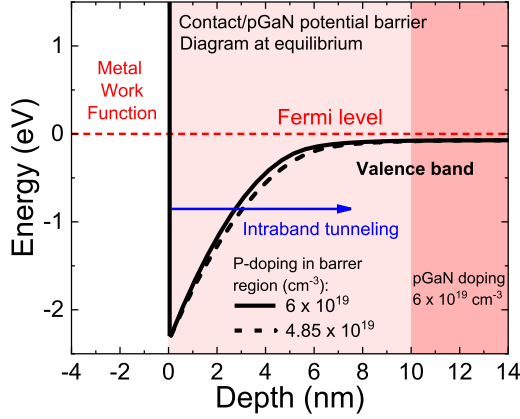


Fig. 3. Simulated band diagram of the p-contact before and after the ageing procedure. Direct tunneling was implemented in the first 10 nm adjacent to the metal where the partial passivation of Mg doping was supposed to occur during stress.

Fig. 3 reports the band diagram of the p-GaN region adjacent to the contact: a potential barrier at the metal/p-GaN interface can be observed, with a height of about 2.2 eV and a width of about 10 nm. These first nanometers of the p-GaN layer are very sensitive to the doping density, since small changes affect the local thickness of the barrier.

Therefore, in the simulation framework we defined the p-contact as a Schottky contact with a work-function equal to 5.1 eV (Pd/Au). Besides, we considered direct tunneling as the dominant injection process since the heavy doping of the GaN layer results a thin barrier [30], and we placed a dense non-local mesh (NLM) extending from the metal contact to the first 10 nm of the p-GaN layer. The computation of the tunneling probabilities is based on the Wentzel–Kramers–Brillouin (WKB) approximation [31], [32]. The initial doping concentration of this layer was set at its nominal value ($6 \times 10^{19} \text{ cm}^{-3}$). Thus, we reached a good reproduction of the initial electrical characteristic at 0 min with $m_t = 0.15 m_0$, in agreement with literature, where this value could be in the range $m_t = 0.08 m_0 - 2.2 m_0$ [33], [34] since it is adopted as a fitting parameter that takes into account also other injection mechanisms such as defect-related tunneling transport [35], [36].

Based on these considerations, to reproduce the I-V curve after the stress, we only decreased the active p-doping concentration in the first 10 nm of p-GaN close to the contact, and adjusted the series resistance according to the values reported in Table I.

In Fig. 3, we can see that the lowering in the active Mg-doping concentration leads to a thickening of the barrier, and to the consequent reduction in the tunneling probability. The effect of this mechanism is an increase in the applied bias to obtain the same carrier injection in the device, that justifies the turn-on voltage shift. Finally, the slight variation in the equivalent series resistance reproduced the increase in the resistivity of the p-side region. As shown in the inset of Fig. 5, we obtained a good matching of the electrical characteristics in region (a).

TABLE II
DEFECT PROPERTIES ESTIMATED BY DLOS MEASUREMENT

| | $E_{T,1}$ | $E_{T,2}$ | $E_{T,3}$ |
|----------------------------|----------------------|--------------------|--------------------|
| E_T (eV) | 0.94 | 3.06 | 3.52 |
| N_T (cm^{-3}) | 1.5×10^{14} | 5×10^{15} | 2×10^{16} |

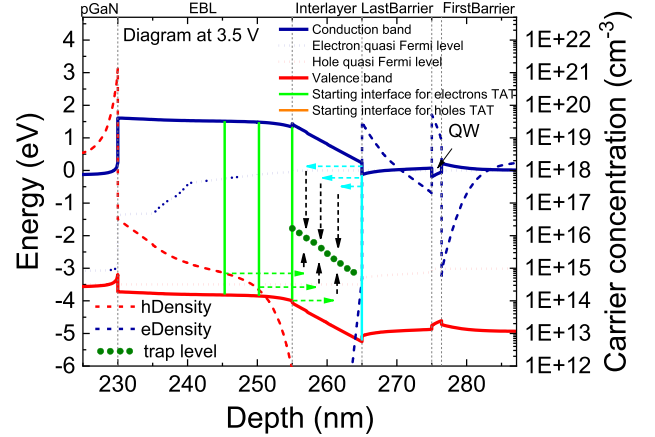


Fig. 4. Simulated band diagram at 3.5 V and schematic representation of the implemented model for TAT.

IV. MODELING OF FORWARD LEAKAGE CURRENT INCREASE

The second process observed during ageing is the increase in the leakage current. Considering that the origin of such process is related to the presence of deep levels within the depletion region, we started our analysis by implementing TAT through the NLMs model proposed by Mandurrino et al., and previously adopted to describe the sub turn-on conduction in visible LEDs [15], [16], [37]. Specifically, a NLM is used to compute the probability of tunneling from a desired starting position toward the traps positioned within a specific device region, according to the equations reported in [15], [37]. Location wise, we found that the undoped interlayer was giving the strongest contribution to TAT. In fact, when the voltage is below turn-on, the free carriers accumulated near this layer have a good energy alignment with the deep-levels; moreover, the short distance from hole- and electron-rich layers favors the TAT mechanisms. Defects located in other regions do not influence the TAT mechanism.

Considering this, we placed traps in the interlayer at $E_C - 3.5 \text{ eV}$. The energy and concentration were estimated by means of deep level optical-spectroscopy (DLOS) measurements [13]. Also other levels were identified collocated at shallower energies, but we proved that only the deeper level gives the main contribution in the leakage current [15]. Table II reports the values of the thermal activation energies (E_T) and of the densities (N_T) estimated before the ageing test.

As reported in Fig. 4, the main electron accumulation is at the interface interlayer/LB; for this reason, we defined a NLM from this region toward the interlayer, optimizing the tunneling probability toward the traps (sky-blue arrows in the figure). Instead, holes are prone to tunnel from the EBL toward the interlayer, but their concentration is orders of magnitude smaller

than that of the electrons. To collect the highest number of holes, we had to define three different starting points in the EBL by means of three NLMs, each of these have a maximum tunneling length of 10 nm, as illustrated by the green arrows in Fig. 4. We set a limitation at 10 nm for the tunneling probability computation, since the contribution for greater distances is negligible [38], [39].

In this configuration, at low voltages, carriers that are energetically aligned with traps can tunnel close to the defects-related levels located in the interlayer, and then recombine through an SRH-like recombination process, [14], [37], [40], [41], thus contributing to the leakage current. The equation that describes the process is the following [31]:

$$R_{TAT} = \frac{N_T c_n c_p (np - n_i^2)}{c_n \left(n + \frac{n_i}{g_n} e^{\frac{E_{T_i}}{k_B T}} \right) + c_p \left(p + \frac{n_i}{g_p} e^{-\frac{E_{T_i}}{k_B T}} \right)}$$

where N_T is the trap density, E_{T_i} is energy level of the traps referred to the intrinsic Fermi level, $g_{n,p}$ are the electron and hole degeneracy factors and $c_{n,p}$ are the capture rates. The latter are given by the combination of two capture/emission mechanisms, a phonon-assisted inelastic process, and an elastic transition. The phonon-assisted transition for electrons from the conduction band is:

$$c_n^{phon} = \frac{g_c V_r S \omega \sqrt{m_t (m_0 k_B T)^3}}{\hbar^3 \sqrt{\chi}} \left(\frac{(S-l)^2}{S} \right) \exp \left[-S(2f+1) + \frac{\Delta E}{2k_B T} + \chi \right] \left(\frac{\gamma}{l+\chi} \right)^l F_{\frac{1}{2}} \left[\frac{E_{F,n} - E_C(0)}{k_B T} \right] \frac{|\Psi(z_0)|^2}{|\Psi(0)|^2}$$

While the elastic transition is obtained by:

$$c_n^{el} = \frac{g_c V_r S \theta \sqrt{8m_t m_0^3}}{\hbar^4 \pi} (E_C(z_0) - E_T)^2 (E_T - E_C(0))^{\frac{3}{2}} F_{\frac{1}{2}} \left[\frac{E_{F,n} - E_T}{k_B T} \right] \frac{|\Psi(z_0)|^2}{|\Psi(0)|^2}$$

where V_T is the interaction volume of the trap, S is the Huang-Rhys factor, $\hbar\omega$ the energy of the phonons involved in the transition (E_{phon}), m_t is the tunneling electron effective mass, g_c is the prefactor for the Richardson constant at the interface, l is the number of the phonons emitted in the transition, f is the Bose-Einstein occupation of the phonon state and finally, $z = 2S\sqrt{f(f+1)}$ and $\chi = \sqrt{l^2 + z^2}$. The dissipated energy in this process is $\Delta E = E_C + \frac{3}{2}k_B T - E_T$. The emission rates are obtained from the capture rates by the principle of detailed balance, whereas the hole terms are analogous to the electrons terms. In the simulations we have set $S = 10$, $V_T = 2 \times 10^{-7} \mu\text{m}^3$ and $\hbar\omega = 91.2 \text{ meV}$ [37].

We obtained the first matching with the I-V curve at 0 min by placing a decreasing trap concentration over the entire interlayer from the EBL toward LB, whose densities at the interfaces are reported in Table I. The table shows also the values adopted for the relative tunneling masses for TAT obtained after an initial calibration. Subsequently, we were able to reach a good

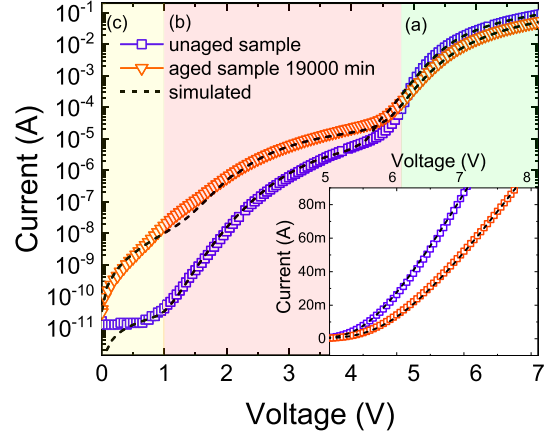


Fig. 5. Comparison between the experimental and the simulated I-V curves before and after the ageing test. Three regions of the electrical characteristic are reproduced by the contact model (a), the trap-assisted tunneling (b) and shunt paths (c). The inset reports the same curves in linear scale.

correspondence with the aged curve by increasing only the defect density in the interlayer and reducing the parasitic shunt resistance (see Fig. 5 the yellow and green region and Table I). From these simulations we found that the main contribution to the forward leakage current is due to TAT. Only after ageing, at voltages lower than 1 V, we have a measurable contribution in the leakage current due to the presence of other parasitic conduction paths [24]. The contribution of this process has been modeled for simplicity by reducing the shunt resistance of the LED, as done also in previous reports [42], [43]. Therefore, these results emulate a stress-induced increase in defects density confirming the hypothesis of the rise in defect concentration in the depletion region during ageing [8], [16], [44].

Furthermore, the trap density, which has a decreasing trend from the EBL/IL interface toward the IL/LB, suggests the presence of a diffusion process. In particular, as reported in the literature by Glaab et al. and Ma et al. [45], [46], [47], by SIMS measurements it is possible to identify a high concentration of hydrogen atoms (above $1 \times 10^{17} \text{ cm}^{-3}$) in the p-type layers, in the EBL and also in the interlayer. This is caused by the incorporation of H ions during growth, even after thermal annealing. During the stress, hydrogen migrates toward the n-side [45], favored by its high thermal diffusion coefficient. The breaking up H-containing defect complexes by hot carriers would cause the activation of point defects within the depletion region [47]. It is worth noticing that the defect densities adopted in the simulations are in accordance with the estimations in Glaab et al.. Nevertheless, further research is necessary to clarify the role of hydrogen and its interaction with the point defects [48], [49]. Anyway, these simulations confirm the hypothesis of trap generation/diffusion in the depletion region from the EBL toward the active region, and provide a useful method to model the degradation processes.

V. SUMMARY AND CONCLUSION

Fig. 5 reports the comparison between the experimental and the simulated measurements. We reached a good matching both in the sub turn-on region, where the TAT-related conduction

dominates, and in the forward bias region, where conduction strongly depends on contact degradation.

In conclusion, we investigated the reliability of a UV-C light-emitting diode through a constant current stress test. Starting from the electrical characteristic before and after stress, we developed a simulation framework capable of describing the observed degradation mechanisms. In particular, we demonstrated by numerical simulations that a contact degradation, consisting in the partial passivation of Mg in the p-GaN region adjacent to the metal, reproduces the shift in the turn-on voltage observed during the ageing. Furthermore, an increase of defects from the EBL toward the active region was found to be responsible for the increase in the forward leakage current. The good matching obtained between the experimental and simulated electrical characteristics ultimately proves that the adopted methodology can be very useful for the identification and modeling of the mechanisms involved in limiting the reliability of UV-C LEDs.

REFERENCES

- [1] W. S. Won et al., "UV-LEDs for the disinfection and bio-sensing applications," *Int. J. Precis. Eng. Manuf.*, vol. 19, pp. 1901–1915, 2018, doi: [10.1007/S12541-018-0218-5](https://doi.org/10.1007/S12541-018-0218-5).
- [2] C. Dreyer and F. Mildner, "Application of LEDs for UV-curing," *Springer Ser. Mater. Sci.*, vol. 227, pp. 415–434, 2016, doi: [10.1007/978-3-319-24100-5_15](https://doi.org/10.1007/978-3-319-24100-5_15).
- [3] M. Schreiner, J. Mar Tí Nez-Abaigar, J. Glaab, and M. Jansen, "UV-B induced secondary plant metabolites," *Opt. Photonik*, vol. 9, pp. 34–37, 2014, doi: [10.1002/OPPH.201400048](https://doi.org/10.1002/OPPH.201400048).
- [4] J. Glaab et al., "Skin tolerant inactivation of multiresistant pathogens using far-UVC LEDs," *Sci. Rep.*, vol. 11, 2021, Art. no. 14647, doi: [10.1038/s41598-021-94070-2](https://doi.org/10.1038/s41598-021-94070-2).
- [5] M. A. Würtele et al., "Application of GaN-based ultraviolet-C light emitting diodes—UV LEDs—for water disinfection," *Water Res.*, vol. 45, pp. 1481–1489, 2011, doi: [10.1016/j.watres.2010.11.015](https://doi.org/10.1016/j.watres.2010.11.015).
- [6] K. Michael and J. Rass, *III-Nitride Ultraviolet Emitters*. Cham, Switzerland: Springer Int. Publishing, 2016, doi: [10.1007/978-3-319-24100-5](https://doi.org/10.1007/978-3-319-24100-5).
- [7] H. Amano et al., "The 2020 UV emitter roadmap," *J. Phys. D Appl. Phys.*, vol. 53, 2020, Art. no. 503001, doi: [10.1088/1361-6463/aba64c](https://doi.org/10.1088/1361-6463/aba64c).
- [8] D. Monti et al., "High-current stress of UV-B (In)AlGaIn-based LEDs: Defect-generation and diffusion processes," *IEEE Trans. Electron Devices*, vol. 66, no. 8, pp. 3387–3392, Aug. 2019, doi: [10.1109/TED.2019.2920521](https://doi.org/10.1109/TED.2019.2920521).
- [9] J. Grandusky, Y. Cui, S. Gibb, M. Mendrick, and L. Schowalter, "Performance and reliability of ultraviolet-C pseudomorphic light emitting diodes on bulk AlN substrates," *Phys. Status Solidi C*, vol. 7, pp. 2199–2201, 2010, doi: [10.1002/PSSC.200983635](https://doi.org/10.1002/PSSC.200983635).
- [10] F. J. Arques-Orobon, N. Nuñez, M. Vazquez, C. Segura-Antunez, and V. González-Posadas, "High-power UV-LED degradation: Continuous and cycled working condition influence," *Solid. State. Electron.*, vol. 111, pp. 111–117, 2015, doi: [10.1016/j.sse.2015.05.039](https://doi.org/10.1016/j.sse.2015.05.039).
- [11] Y. Z. Wang et al., "Degradation in AlGaIn-based UV-C LEDs under constant current stress: A study on defect behaviors," *Appl. Phys. Lett.*, vol. 116, 2020, Art. no. 203501, doi: [10.1063/5.0010540](https://doi.org/10.1063/5.0010540).
- [12] N. Susilo et al., "Improved performance of UVC-LEDs by combination of high-temperature annealing and epitaxially laterally overgrown AlN/sapphire," *Photon. Res.*, vol. 8, pp. 589–594, 2020, doi: [10.1364/PRJ.385275](https://doi.org/10.1364/PRJ.385275).
- [13] N. Roccato et al., "Modeling the electrical degradation of AlGaIn-based UV-C LEDs by combined deep-level optical spectroscopy and TCAD simulations," *Appl. Phys. Lett.*, vol. 122, 2023, Art. no. 161105, doi: [10.1063/5.0144721/2884739](https://doi.org/10.1063/5.0144721/2884739).
- [14] M. Mandurrino et al., "Semiclassical simulation of trap-assisted tunneling in GaN-based light-emitting diodes," *J. Comput. Electron.*, vol. 14, pp. 444–455, 2015, doi: [10.1007/s10825-015-0675-3](https://doi.org/10.1007/s10825-015-0675-3).
- [15] N. Roccato et al., "Modeling the electrical characteristics of InGaIn/GaN LED structures based on experimentally-measured defect characteristics," *J. Phys. D. Appl. Phys.*, vol. 54, 2021, Art. no. 425105, doi: [10.1088/1361-6463/AC16FD](https://doi.org/10.1088/1361-6463/AC16FD).
- [16] N. Roccato et al., "Modeling the electrical characteristic of InGaIn/GaN blue-violet LED structure under electrical stress," *Microelectron. Reliab.*, vol. 138, 2022, Art. no. 114724, doi: [10.1016/J.MICROREL.2022.114724](https://doi.org/10.1016/J.MICROREL.2022.114724).
- [17] C. Z. Zhao, T. Wei, L. Y. Chen, S. S. Wang, and J. Wang, "The activation energy for Mg acceptor in AlGa1-xN alloys in the whole composition range," *Superlattices Microstruct.*, vol. 109, pp. 758–762, 2017, doi: [10.1016/j.spmi.2017.06.006](https://doi.org/10.1016/j.spmi.2017.06.006).
- [18] Y. Nakano and T. Jimbo, "Electrical properties of acceptor levels in Mg-doped GaN," *Phys. Status Solidi*, pp. 438–442, 2003, doi: [10.1002/pssc.200390082](https://doi.org/10.1002/pssc.200390082).
- [19] L. Silvestri, K. Dunn, S. Prawer, and F. Ladouceur, "Hybrid functional study of Si and O donors in wurtzite AlN," *Appl. Phys. Lett.*, vol. 99, 2011, Art. no. 122109, doi: [10.1063/1.3641861](https://doi.org/10.1063/1.3641861).
- [20] R. Ni, Z. Yu, Z. Liu, L. Zhang, L. Jia, and Y. Zhang, "Light extraction and Auger recombination in AlGaIn-based ultraviolet Light-emitting diodes," *IEEE Photon. Technol. Lett.*, vol. 32, no. 16, pp. 971–974, Aug. 2020, doi: [10.1109/LPT.2020.3006863](https://doi.org/10.1109/LPT.2020.3006863).
- [21] F. Nippert et al., "Auger recombination in AlGaIn quantum wells for UV light-emitting diodes," *Appl. Phys. Lett.*, vol. 113, 2018, Art. no. 071107, doi: [10.1063/1.5044383](https://doi.org/10.1063/1.5044383).
- [22] P. Pampili and P. J. Parbrook, "Doping of III-nitride materials," *Mater. Sci. Semicond. Process.*, vol. 62, pp. 180–191, 2017, doi: [10.1016/J.MSSP.2016.11.006](https://doi.org/10.1016/J.MSSP.2016.11.006).
- [23] A. Muhin et al., "Radiative recombination and carrier injection efficiencies in 265 nm deep ultraviolet light-emitting diodes grown on AlN/sapphire templates with different defect densities," *Phys. Status Solidi*, vol. 220, 2023, Art. no. 2200458, doi: [10.1002/PSSA.202200458](https://doi.org/10.1002/PSSA.202200458).
- [24] L. Liu, M. Ling, J. Yang, W. Xiong, W. Jia, and G. Wang, "Efficiency degradation behaviors of current/thermal co-stressed GaN-based blue light emitting diodes with vertical-structure," *J. Appl. Phys.*, vol. 111, 2012, Art. no. 093110, doi: [10.1063/1.4712030](https://doi.org/10.1063/1.4712030).
- [25] R. Nana et al., "Effect of deep-level states on current-voltage characteristics and electroluminescence of blue and UV light-emitting diodes," *Phys. Status Solidi*, vol. 207, pp. 1489–1496, 2010, doi: [10.1002/PSSA.200925596](https://doi.org/10.1002/PSSA.200925596).
- [26] J. H. Park, J. K. Kim, and J. Cho, "Observation of space-charge-limited current in AlGaIn/GaN ultraviolet light-emitting diodes," *Mater. Lett.*, vol. 214, pp. 217–219, 2018, doi: [10.1016/J.MATLET.2017.12.011](https://doi.org/10.1016/J.MATLET.2017.12.011).
- [27] M. Meneghini et al., "High-temperature degradation of GaN LEDs related to passivation," *IEEE Trans. Electron Devices*, vol. 53, no. 12, pp. 2981–2986, Dec. 2006, doi: [10.1109/TED.2006.885544](https://doi.org/10.1109/TED.2006.885544).
- [28] C. De Santi, A. Caria, F. Piva, G. Meneghesso, E. Zanoni, and M. Meneghini, "Degradation mechanisms of InGaIn visible LEDs and AlGaIn UV LEDs," *Reliab. Semicond. Lasers Optoelectron. Devices*, vol. 2021, pp. 273–312, 2021, doi: [10.1016/B978-0-12-819254-2.00001-1](https://doi.org/10.1016/B978-0-12-819254-2.00001-1).
- [29] L. Trevisanello, M. Meneghini, U. Zehnder, B. Hahn, G. Meneghesso, and E. Zanoni, "High temperature instabilities of ohmic contacts on p-GaN," *Phys. Status Solidi C*, vol. 5, pp. 435–440, 2008, doi: [10.1002/PSSC.200777475](https://doi.org/10.1002/PSSC.200777475).
- [30] G. Greco, F. Iucolano, and F. Roccaforte, "Ohmic contacts to gallium nitride materials," *Appl. Surf. Sci.*, vol. 383, pp. 324–345, 2016, doi: [10.1016/J.APSUSC.2016.04.016](https://doi.org/10.1016/J.APSUSC.2016.04.016).
- [31] Synopsys, Inc., "SentaurusTM device user guide," 2015. [Online]. Available: <http://www.synopsys.com/Company/Pages/Trademarks.aspx>
- [32] Z. H. Huang, T. E. Feuchtwang, P. H. Cutler, and E. Kazes, "Wentzel-Kramers-Brillouin method in multidimensional tunneling," *Phys. Rev. A*, vol. 41, 1990, Art. no. 32, doi: [10.1103/PhysRevA.41.32](https://doi.org/10.1103/PhysRevA.41.32).
- [33] B. Santi, "On the hole effective mass and the free hole statistics in wurtzite GaN," *Semicond. Sci. Technol.*, vol. 18, pp. 219–224, 2003.
- [34] M. Auf Der Maur, B. Galler, I. Pietzonka, M. Strassburg, H. Lugauer, and A. Di Carlo, "Trap-assisted tunneling in InGaIn single-quantum-well light-emitting diodes," *Appl. Phys. Lett.*, vol. 105, 2014, Art. no. 133504, doi: [10.1063/1.4896970](https://doi.org/10.1063/1.4896970).
- [35] M. B. Gonzalez, G. Eneman, G. Wang, B. De Jaeger, E. Simoen, and C. Claeys, "Analysis of the temperature dependence of trap-assisted tunneling in Ge pFET junctions," *J. Electrochem. Soc.*, vol. 158, 2011, Art. no. H955, doi: [10.1149/1.3614518](https://doi.org/10.1149/1.3614518).
- [36] H. Zhang, E. J. Miller, and E. T. Yu, "Analysis of leakage current mechanisms in Schottky contacts to GaN and Al_{0.25}Ga_{0.75}N/GaN grown by molecular-beam epitaxy," *J. Appl. Phys.*, vol. 99, 2006, Art. no. 023703, doi: [10.1063/1.2159547](https://doi.org/10.1063/1.2159547).
- [37] M. Mandurrino et al., "Physics-based modeling and experimental implications of trap-assisted tunneling in InGaIn/GaN light-emitting diodes," *Phys. Status Solidi*, vol. 212, pp. 947–953, 2015, doi: [10.1002/pssa.201431743](https://doi.org/10.1002/pssa.201431743).

- [38] S. Krishnamoorthy, D. N. Nath, F. Akyol, P. S. Park, M. Esposto, and S. Rajan, "Polarization-engineered GaN/InGaN/GaN tunnel diodes," *Appl. Phys. Lett.*, vol. 97, 2010, Art. no. 203502, doi: [10.1063/1.3517481](https://doi.org/10.1063/1.3517481).
- [39] S. Krishnamoorthy, F. Akyol, P. S. Park, and S. Rajan, "Low resistance GaN/InGaN/GaN tunnel junctions," *Appl. Phys. Lett.*, vol. 102, 2013, Art. no. 113503, doi: [10.1063/1.4796041](https://doi.org/10.1063/1.4796041).
- [40] F. Jiménez-Molinos, F. Gámiz, A. Palma, P. Cartujo, and J. A. López-Villanueva, "Direct and trap-assisted elastic tunneling through ultrathin gate oxides," *J. Appl. Phys.*, vol. 91, pp. 5116–5124, 2002, doi: [10.1063/1.1461062](https://doi.org/10.1063/1.1461062).
- [41] Synopsys, Inc, *Sentaurus™ Structure Ed. User Guide Destination Control Statement*, 2015. Accessed: Jul. 30, 2020. [Online]. Available: <http://www.synopsys.com/Company/Pages/Trademarks.aspx</bib>>
- [42] M. W. Moseley, A. A. Allerman, M. H. Crawford, J. J. Wierer, M. L. Smith, and A. M. Armstrong, "Detection and modeling of leakage current in AlGaIn-based deep ultraviolet light-emitting diodes," *J. Appl. Phys.*, vol. 117, 2015, Art. no. 095301, doi: [10.1063/1.4908543](https://doi.org/10.1063/1.4908543).
- [43] T. Tao et al., "Observation and modeling of leakage current in AlGaIn ultraviolet light emitting diodes," *IEEE Photon. Technol. Lett.*, vol. 31, no. 21, pp. 1697–1700, Nov. 2019, doi: [10.1109/LPT.2019.2942612](https://doi.org/10.1109/LPT.2019.2942612).
- [44] F. Piva et al., "Modeling the degradation mechanisms of AlGaIn-based UVC LEDs: From injection efficiency to mid-gap state generation," *Photon. Res.*, vol. 8, pp. 1786–1791, 2020, doi: [10.1364/PRJ.401785](https://doi.org/10.1364/PRJ.401785).
- [45] J. Glaab et al., "Degradation of (In)AlGaIn-based UVB LEDs and migration of hydrogen," *IEEE Photon. Technol. Lett.*, vol. 31, no. 7, pp. 529–532, Apr. 2019, doi: [10.1109/LPT.2019.2900156](https://doi.org/10.1109/LPT.2019.2900156).
- [46] Z. Ma, H. Cao, S. Lin, X. Li, and L. Zhao, "Degradation and failure mechanism of AlGaIn-based UVC-LEDs," *Solid. State. Electron.*, vol. 156, pp. 92–96, 2019, doi: [10.1016/J.SSE.2019.01.004](https://doi.org/10.1016/J.SSE.2019.01.004).
- [47] J. Glaab et al., "Impact of operation parameters on the degradation of 233 nm AlGaIn-based far-UVC LEDs," *J. Appl. Phys.*, vol. 131, 2022, Art. no. 014501, doi: [10.1063/5.0069590](https://doi.org/10.1063/5.0069590).
- [48] M. Meneghini et al., "Defect-related degradation of deep-UV-LEDs," *Microelectron. Reliab.*, vol. 50, pp. 1538–1542, 2010, doi: [10.1016/j.microrel.2010.07.089](https://doi.org/10.1016/j.microrel.2010.07.089).
- [49] S. F. Chichibu et al., "Operation-induced degradation mechanisms of 275-nm-band AlGaIn-based deep-ultraviolet light-emitting diodes fabricated on a sapphire substrate," *Appl. Phys. Lett.*, vol. 122, 2023, Art. no. 201105, doi: [10.1063/5.0147984/2891410](https://doi.org/10.1063/5.0147984/2891410).